



Dalton  
Transactions

**Modifying the Internal Substituents of Self-Assembled  
Cages Controls their Molecular Recognition and Optical  
Properties**

Journal:	<i>Dalton Transactions</i>
Manuscript ID	DT-ART-05-2022-001451.R1
Article Type:	Paper
Date Submitted by the Author:	15-Jun-2022
Complete List of Authors:	Woods, Connor; UCR, Chemistry Wu, Hoi-Ting; UCR, Chemistry Ngai, Courtney; UCR, Chemistry da Camara, Bryce; UCR, Chemistry Julian, Ryan; University of California Riverside, Hooley, Richard; UCR, Chemistry

SCHOLARONE™  
Manuscripts

## Modifying the Internal Substituents of Self-Assembled Cages Controls their Molecular Recognition and Optical Properties

Connor Z. Woods, Hoi-Ting Wu, Courtney Ngai, Bryce da Camara, Ryan R. Julian and Richard J. Hooley\*

Received 00th January 20xx,  
Accepted 00th January 20xx

DOI: 10.1039/x0xx00000x

www.rsc.org/

Self-assembled  $\text{Fe}_4\text{L}_6$  cage complexes with variable internal functions can be synthesized from a 2,7-dibromocarbazole ligand scaffold, which orients six functional groups to the cage interior. Both ethylthiomethylether and ethyldimethylamino groups can be incorporated. The cages show strong ligand-centered fluorescence emission and a broad range of guest binding properties. Coencapsulation of neutral organic guests is favored in the larger, unfunctionalized cage cavity, whereas the thioether cage has a more sterically hindered cavity that favors 1:1 guest binding. Binding affinities up to  $10^6 \text{ M}^{-1}$  in  $\text{CH}_3\text{CN}$  are seen. The dimethylamino cage is more complex, as the internal amines display partial protonation and can be deprotonated by amine bases. This amine cage displays affinity for a broad range of neutral organic substrates, with affinities and stoichiometries comparable to that of the similarly sized thioether cage. These species show that simple variations in ligand backbone allow variations in the number and type of functions that can be displayed towards the cavity of self-assembled hosts, which will have applications in biomimetic sensing, catalysis and molecular recognition.

### Introduction

Self-assembled metal-ligand coordination cages<sup>1</sup> have a variety of uses, from molecular recognition<sup>2</sup> and catalysis<sup>3</sup> to cargo delivery<sup>4</sup> and sensing.<sup>5</sup> The inspiration for these systems has long been that of natural proteins and enzymes: species with a defined cavity capable of selective molecular recognition. The major difference between the active sites of enzymes and that of self-assembled coordination cages is that enzymes display reactive functional groups towards the active site cavity, but that is far less common for synthetic mimics. There are a number of obstacles to introducing reactive functional groups to self-assembled cages:<sup>7</sup> the functions can be incompatible with the assembly process, occupy the internal cavity (and limit guest recognition) or simply fail to be oriented in the correct direction (i.e. externally, rather than internally). Despite these challenges, a number of cage complexes have been created that orient reactive functional groups towards internal cavities.<sup>8</sup> These cages have been exploited for selective catalysis,<sup>8c,d</sup> including sequential tandem catalysis,<sup>8f</sup> as well as for the recognition of challenging targets.<sup>8g</sup> One limitation, however, is the scope of groups that can be incorporated: inert groups are simple to add,<sup>8a,b</sup> and acidic groups are moderately well-tolerated,<sup>8c,d,f, 9a-c</sup> but strongly basic lone pairs such as amines are still a challenge.<sup>8f</sup>

#### Internally Functionalized Self-assembled $\text{Fe}_4\text{L}_6$ Cages

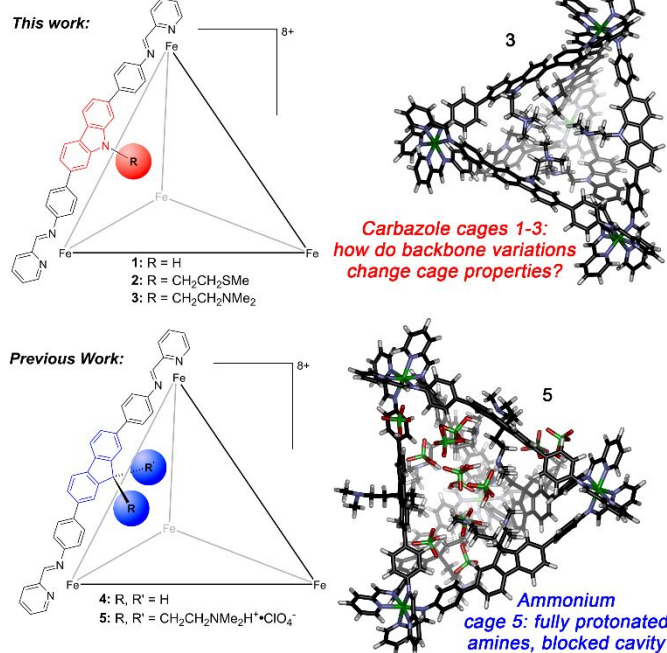


Figure 1. Internally functionalized self-assembled  $\text{Fe}^{\text{II}}_4\text{L}_6$  cages discussed in this work.

We have previously described the synthesis, molecular recognition and catalytic properties of a series of  $\text{Fe}^{\text{II}}_4\text{L}_6$  cages with internalized functional groups, based on a 2,7-diarylfuorene scaffold.<sup>9</sup> The slightly bent, V-shaped ligands allow internalization of groups such as carboxylic acids<sup>9a-c</sup> or dimethylamino groups,<sup>9d</sup> while retaining the ability to form  $\text{M}_4\text{L}_6$  tetrahedra with a cavity that is capable of binding and

\*Department of Chemistry, University of California - Riverside, Riverside, CA 92521, USA. E-mail: richard.hooley@ucr.edu.

† Electronic Supplementary Information (ESI) available: New molecule characterization; spectral data not included in the text, including NMR, UV/Vis and fluorescence emission spectra. See DOI: 10.1039/x0xx00000x

activating multiple different species on the interior. The 2,7-diarylfluorene scaffold displays 12 of these groups on the cage interior (two from each ligand), and while assembly is still possible with this level of internal packing, it does limit the types of functional groups that can be positioned on the cage interior. As such, we began investigating other ligand backbone scaffolds that would retain the geometrical properties of the successful fluorene-based ligands, but allow incorporation of fewer (and more varied) internal groups. Here we describe the synthesis of a series of  $M_4L_6$  tetrahedra (**1-3**, Figure 1) using a 2,7-diarylcarbazole scaffold, analyze their optical and molecular recognition properties, and highlight differences in function by varying the number of functional groups on the cage interiors.

A specific advantage of incorporating fewer groups on the cage interior can be seen when comparing the structure of **1-3** to that of the recently published cage **5**,<sup>9d</sup> which displayed 12 dimethylamino groups on the interior. In that case, the assembly process was only successful if the amines were fully protonated, a side product of which was that the cavity was blocked by  $ClO_4^-$  ions. Tailoring the cage interior will allow a greater range of substrate recognition and, potentially, base-mediated catalysis.

## Results and Discussion

The initial task was to test whether the carbazole ligand core could be suitably functionalized, while still assembling into the desired  $M_4L_6$  structure and positioning the functional groups towards the cage interior. While the carbazole scaffold was enticing, due to its identical geometry and rigidity (compared the fluorenyl scaffold in **4**, **5**), it introduced some synthetic challenges in the functionalization. The carbazole group was prone to either E2 or E1cb elimination in the presence of bases, so while groups such as  $-CH_2CO_2Et$  could be added to 2,7-dibromocarbazole **A**, retaining these groups through the subsequent steps proved challenging. In addition, appending groups such as  $-(CH_2)_3SO_3H$  reduced the solubility of the carbazole ligands to such an extent that self-assembly was unsuccessful. However, reaction of nitrogen or sulfur mustards with **A** proved successful (Figure 2). The conditions were surprisingly finicky, and only a phase-transfer process using NaOH and  $Bu_4N \cdot HSO_4$  gave the functionalized carbazoles in useful yields. Addition of chloroethylmethylsulfide was simple, resulting in precursor **B** in 94% yield, but the formation of the nitrogen equivalent **C** was only possible using the hydrochloride salt of chloroethyl dimethylamine, and even then, in only 63% yield. Extension of these ligand interiors *via* our standard Suzuki process using 4-Boc-aminophenylboronic acid was successful in each case. After deprotection with  $CF_3COOH$ , three dianiline ligands **L1-L3** could be accessed in moderate, but sufficient yield to test their suitability for multicomponent self-assembly.

The first self-assembly test involved the unfunctionalized carbazole ligand **L1**. Combining **L1** with  $Fe(NTf_2)_2$  and 2-formylpyridine (PyCHO, Figure 2) followed by reflux in  $CH_3CN$  for 24 h gave carbazole cage **1** as a ruby red solid in 52% yield. As the carbazole backbone formed cage **1** in a manner that was very similar to that of the known fluorene equivalent **4**, we

tested the more complex ligands **L2** and **L3**. As both **L2** and **L3** contain functions that can competitively coordinate with the Fe salts during assembly, a series of reaction conditions were screened for both. Gratifyingly, cage **2** formed smoothly with  $Fe(NTf_2)_2$  and PyCHO, despite the presence of the sulfide group on the ligand. Notably, the yield of **2** was maximized (47%) with a slight excess of  $Fe(NTf_2)_2$  over the required  $M_4L_6$  stoichiometry, presumably to compensate for some metal coordination by the sulfide groups, and the assembly was performed under rigorously air-free conditions.

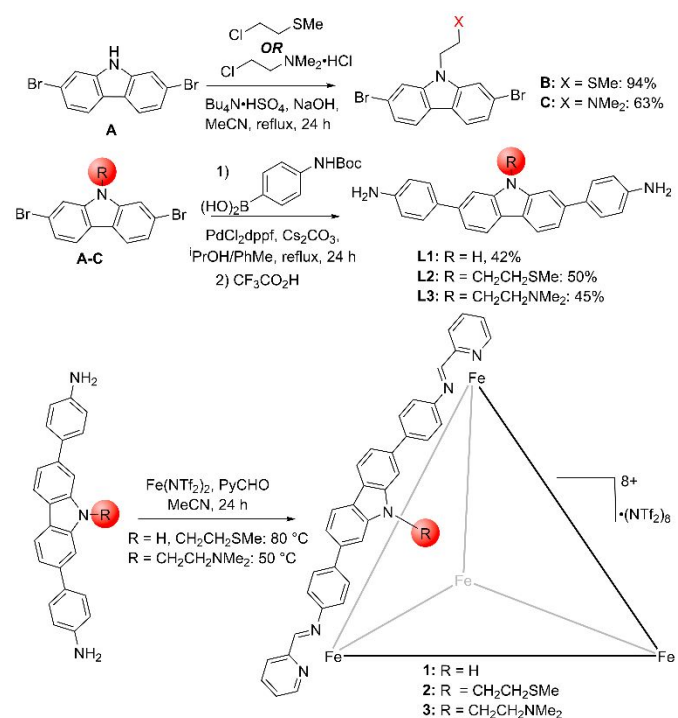
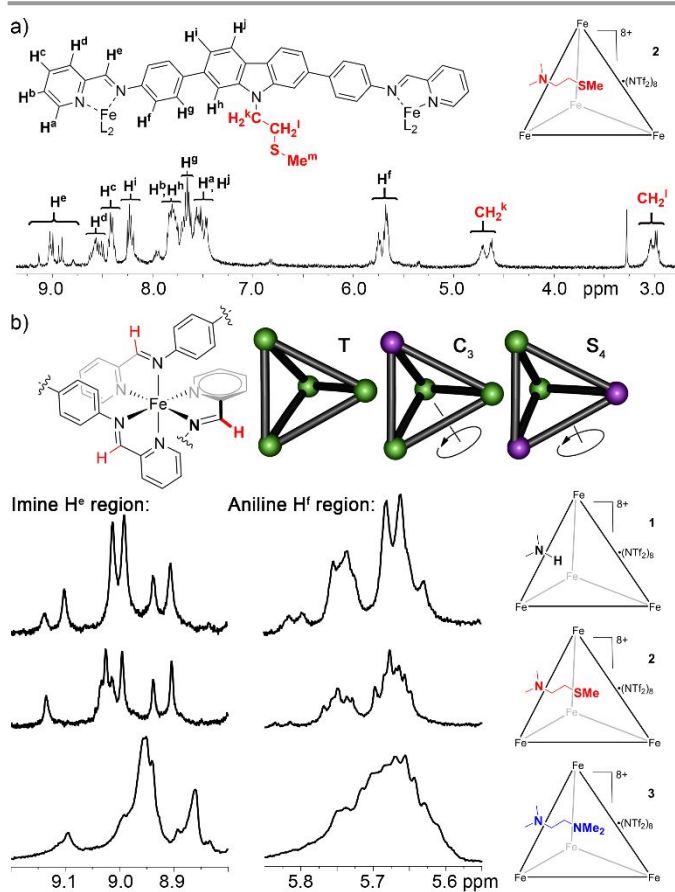


Figure 2. Ligand synthesis and multicomponent assembly of carbazole cages **1-3**.

While the sulfide groups in ligand **L2** only showed weak coordination to the Fe centers and minimal interference in the assembly process, introducing more basic amino groups to the ligand provides a far greater challenge. Basic groups are often poorly tolerated in the self-assembly process, and even though **L3** contains an R-NMe<sub>2</sub> group (to avoid transimination of the iminopyridine groups in the assembly<sup>10</sup>), there are very few examples of self-assembled metal-ligand cages that display basic amines on the interior.<sup>8f,9d,11</sup> The recently published cage **5**<sup>9d</sup> only formed under highly specific reaction conditions, using excess metal, specifically  $Fe(ClO_4)_2$ , with  $Fe(NTf_2)_2$  proving unsuccessful. Fortunately, the formation of cage **3** was possible using only slightly modified conditions to those used for **1** and **2**. The reaction was successful using either  $Fe(NTf_2)_2$  or  $Fe(ClO_4)_2$ , with a slight excess of metal giving the best yield (55%). The reaction temperature was lowered to 50 °C to limit cage decomposition during the assembly process, as the amine cage **3** was less stable than either **1** or **2**. Cages **1-3** were analyzed by 1D and 2D NMR techniques, and ESI-MS. As cages **1-3** are large and complex with substantial void space, form as mixtures of isomers and (in two cases) contain basic groups, we

were unsuccessful in growing X-ray quality crystals. However, the  $^1\text{H}$  NMR spectra were all generally reminiscent of the well-characterized fluorene cages **4-6**, with the imine regions ( $\sim 9.0$  ppm) and aniline CH regions ( $\sim 5.7$  ppm) showing clear evidence of peak splitting into multiple isomers of  $\text{M}_4\text{L}_6$  tetrahedra (Figure 3a for cage **2**, for full spectra of cages **1-3**, see ESI). Cages **1** and **2** displayed quite similar isomer mixture ratios, as can be seen by the splitting of the imine ( $\text{H}^e$ ) and aniline ( $\text{H}^f$ ) proton regions. The  $S_4/C_3/T$  ratio can only be roughly estimated due to peak overlap, but is  $\sim 50:45:5$ , similar to that shown by **4**.<sup>9a</sup> The prevalence of two isomers can be seen most clearly in the peaks for the internal  $-\text{CH}_2\text{CH}_2-\text{SMe}$ , as the methylenes ( $\text{CH}_2^k$ ) each display two multiplets of approximately equal intensity. 2D DOSY spectra for cages **1-3** (see ESI) indicated that the peak multiplicity was due to isomers of the  $\text{M}_4\text{L}_6$  structure, as each peak showed diffusion at identical rates, indicating they belong to species of the same assembly stoichiometry.



**Figure 3.** NMR analysis of cages **1-3**. a) Assigned  $^1\text{H}$  NMR spectrum of cage **2** (the  $\text{SMe}$  group resides under the  $\text{CD}_3\text{CN}$  solvent impurity peak, see ESI); b) expansions of the imine ( $\text{H}^e$ ) and aniline ( $\text{H}^f$ ) proton regions in the  $^1\text{H}$  NMR spectra of **1-3**, to illustrate the isomers observed.  $\text{CD}_3\text{CN}$ , 600 MHz, 298 K.

In contrast, the cage peaks for the amino variant **3** were quite broad (Figure 3b), although the representative peaks for the  $\text{M}_4\text{L}_6$  tetrahedra were present at similar chemical shifts to those of **2**. Analysis of the 2D spectra allowed assignment of the peaks, indicating the presence of six  $\text{CH}_2\text{CH}_2\text{NMe}_2$  groups in the assembly. The broad  $^1\text{H}$  NMR spectrum provided another piece of evidence that the hexa-amino cage **3** behaves differently

than the dodeca-ammonium cage **5**, which showed very sharp cage peaks in the  $^1\text{H}$  NMR, with each of the  $\text{NMe}_2\text{H}^+$  methyl peaks split into doublets, due to scalar coupling between the methyl groups and a strongly coordinated proton on each nitrogen atom. In contrast, the ligand backbone peaks for  $(\mathbf{3}\cdot\text{NTf}_2)_8$  were broadened, and the  $\text{NMe}_2$  peaks resided at 2.8-2.6 ppm and were broad singlets. No evidence for strong, persistent formation of  $\text{NMe}_2\text{H}^+$  ions on the interior could be seen: no crosspeaks were present between the  $\text{NMe}_2$  resonances and any other protons in either the 2D COSY or 2D NOESY spectra (ESI Figures S-37 and S-40).

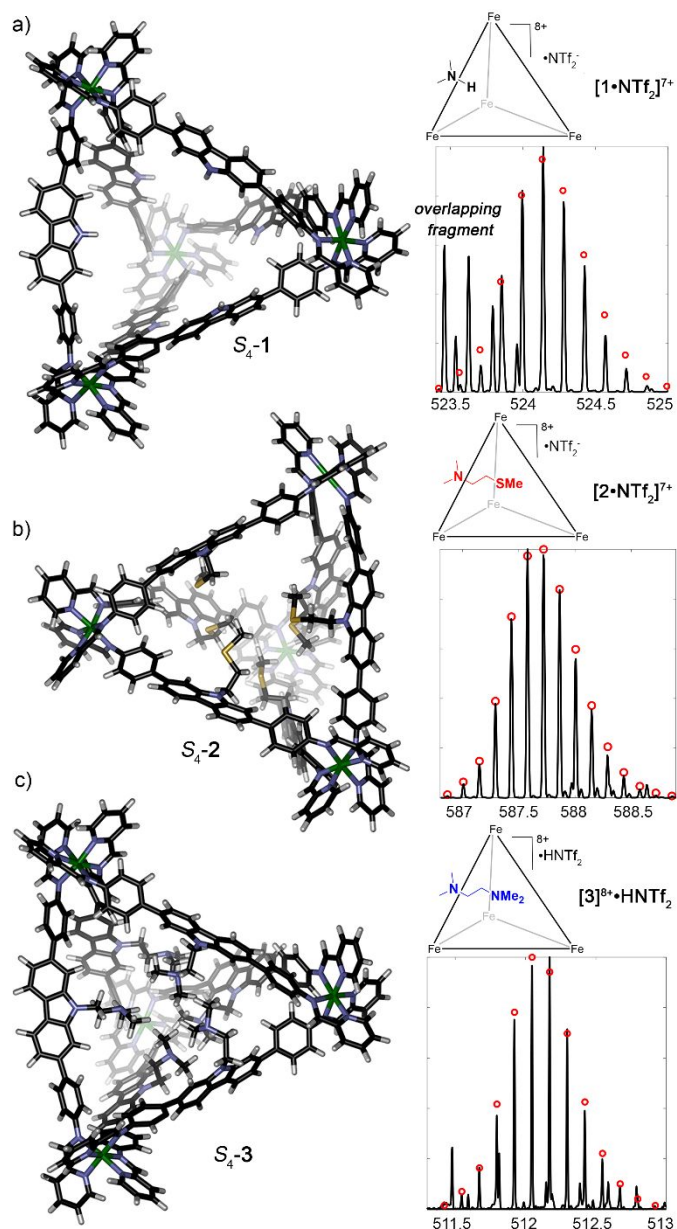


**Figure 4.** Minimized structures and observed isotope patterns for  $\text{M}_4\text{L}_6$  ions observed in the ESI-MS spectra of cages a) **1**; b) **2**; c) **3** (red dots = theoretical peak intensities for the calculated isotope patterns).

The three new cages **1-3** were analyzed by nanoESI-MS, using direct injection of 100%  $\text{CH}_3\text{CN}$  solution of cage into a Thermo Fisher Orbitrap Velos Pro mass spectrometer with a homebuilt

nanoESI source. The spray voltage, capillary temperature, and the S-lens RF level were tuned to achieve maximum signal for the assembled  $M_4L_6$  structures, as the cages were prone to significant fragmentation, far more so than the previously analyzed cages **4-5**. However, after optimization, parent  $M^+$  peaks for the  $[Fe_4L_6]^{8+}$  ions could be observed for all three cages, and matched with predicted isotope patterns (Figure 4). The fragility of the cages, and the presence of multiple isomers of cage, prevented successful growth of X-Ray quality crystals, but the  $M_4L_6$  assemblies were analyzed by molecular minimization (SPARTAN, Hartree-Fock), and the structures of the  $S_4$  isomers of each cage (**1-3**) are shown in Figure 4.

The ESI-MS analysis of **1** and **2** was as expected, and provides supporting evidence for the  $M_4L_6$  structures of the cages. The cages (especially unfunctionalized carbazole **1**) were highly prone to fragmentation, but the  $[1/2]^{8+}$  ions could be isolated and identified by their isotope patterns (red dots in Figure 4). Other important observed ions consisted of  $NH_2^+$  adducts of the  $[M_4L_6]^{8+}$  ions. However, the ions observed for amine cage **3** were slightly different, and more careful investigation of the ESI-MS spectra of **3** and **5** sheds light on the differences between the two amine cages, as well as the differences between the amine cage **3** and the less/non-basic cages **2** and **1** (Figure 5). Dodeca-ammonium cage **5** shows only a very small peak cluster for the  $[Fe_4L_6]^{8+}$  ion,<sup>9d</sup> nor are there appreciable peaks for the  $[5 \cdot ClO_4]^{7+}$ , or  $[5 \cdot (ClO_4)_2]^{6+}$  ions. Instead, as can be seen in Figure 5b, a series of 8+ ions with varying numbers of  $HClO_4$  molecules present can be seen, i.e.  $[5]^{8+} \cdot nHClO_4$ , with  $n$  ranging from 3-8 (Figure 5b). The strong protonation of the cage in solution persists in the ESI-MS spectrum, with sequential loss of  $HClO_4$  molecules observed. In contrast, the ESI-MS spectrum for hexa-amine cage **3** shows much less evidence for protonation. The  $[3]^{8+}$  ion is the most intense  $M_4L_6$  peak, and while some protonated adducts are observed (e.g.  $[3]^{8+} \cdot HNTf_2$  -  $[3]^{8+} \cdot 3HNTf_2$ , they are smaller than the  $[3]^{8+}$  ion and less dominant, accompanied by other fragmentation peaks. This mirrors the NMR data, suggesting that the amines in **3** are not globally protonated (as was the case for **5**), and free amine lone pairs are present in this particular cage.

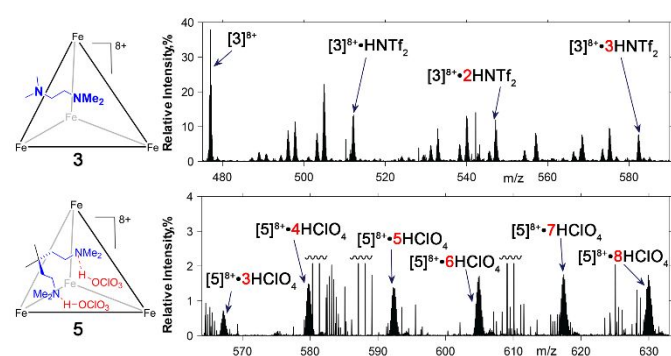


**Figure 5.** Comparison between the ESI-MS spectra of cages **3** and **5**, illustrating the different cage protonation states observed.

The nature of the internal space of cages **1-3** was further investigated by fluorescence spectroscopy, and a UV-Vis analysis of their molecular recognition properties. All five cages

show fluorescence emission spectra when excited at either UV maxima of 265 or 340 nm, corresponding to ligand-centered emission. While the fluorenyl cages **4** and **5** show weak MLCT bands at 575 nm, these absorptions are smaller in the carbazole variants **1-3** (see ESI). No emission is observed upon excitation at 575 in each case, presumably due to rapid collapse of the  $Fe^{II}$  MLCT excited state. Figure 6 shows the normalized emission spectra for cages **1-5** when excited at 340 nm: the emission maxima for cages **1-4** are all quite similar, around  $425 \pm 5$  nm, whereas cage **5** is blue-shifted by 25 nm. The strongest intensity emission is shown by thioether cage **2**, but the most important difference, is the relative intensity of **5** vs **3**. The presence of amine lone pairs is well-known to quench emission, and this quenching can be turned off with protonation.<sup>12</sup> Ammonium cage **5** has a higher emission intensity than **4**, because the amine lone pairs are fully saturated, so are unable to quench the emission. In contrast, the emission intensity of **3** is only 30% that of **2**, and 50% that of **1**. This reinforces the NMR and MS data, showing that only partial protonation of the lone pairs is seen in **3**, and the remaining lone pairs are capable of quenching the emission from the cage complex.

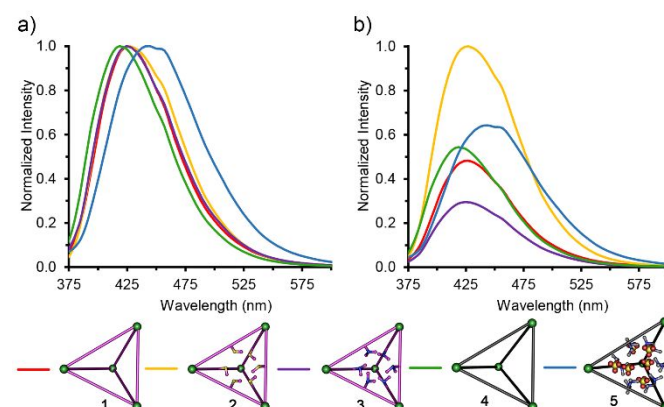


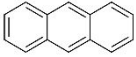
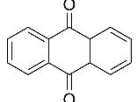
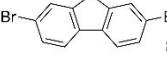
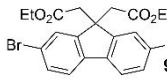
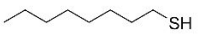
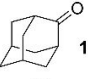
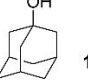
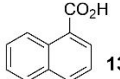
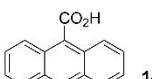
**Figure 6.** Emission spectra of cages **1-5**, a) normalized by intensity to illustrate  $\lambda_{em}$  differences; b) relative emission intensity normalized to cage **2**.  $\lambda_{ex} = 340$  nm,  $CH_3CN$ ,  $[1-5] = 1.0 \mu M$ .

The molecular recognition properties of cages **1-3** were analyzed and compared to those of fluorene cage **4** (which have been extensively studied before<sup>13</sup>) and ammonium cage **5**. UV-Vis absorbance analysis is the most effective method of determining binding affinities in these cages, as neutral guests show fast in/out rates and do not tend to form long-lasting Michaelis complexes that can easily be seen in  $^1H$  NMR. In addition, as the binding is quite remote from the ligand protons, only small shifts in the  $^1H$  NMR are seen.<sup>9</sup> In contrast, large changes in UV absorbance can be seen upon titration of neutral guests into 1.0  $\mu M$  solutions of cage in  $CH_3CN$  (Figure 7, ESI Figures S-49 - S-56). A series of guests were titrated into cages **1-3** (Table 1), and the change in cage absorbance measured at two frequencies, 325 nm and 365 nm (either side of the isosbestic point), and the affinities calculated *via* the Nelder-Mead method.<sup>14</sup> As cages **1-3** can all ostensibly bind multiple species in their large cavities (as has been seen with **4**<sup>13</sup>), 1:1 and 1:2 binding models were tested in each case, and both  $K_a$

(1:1) and  $K_{11}/K_{12}$  (1:2) are reported here, unless the results showed significant error from a poor fit (see ESI for complete results). The guests **6-14** ranged in structure from large, flat aromatics, to alkanethiols and spherical adamantyl derivatives, as well as aromatic acids (naphthoic and anthroic acid). The

range was chosen to allow comparison to previously determined affinities of these guests with **4**.<sup>13</sup> In addition, other small acids (mesic and pivalic acids) and bases (DABCO) were added to cage **3** to analyze the acid-base properties of the putatively basic amine cage.

**Table 1.** Binding constants for neutral guests in cages **1-3**.<sup>a</sup>

Guest	Cage 1		Cage 2		Cage 3	
	$K_a(1:1), \times 10^3 \text{ M}^{-1}$	$K_{11}, K_{12}, \times 10^3 \text{ M}^{-1}$	$K_a(1:1), \times 10^3 \text{ M}^{-1}$	$K_{11}, K_{12}, \times 10^3 \text{ M}^{-1}$	$K_a(1:1), \times 10^3 \text{ M}^{-1}$	$K_{11}, K_{12}, \times 10^3 \text{ M}^{-1}$
 <b>6</b>	120 ± 6.8	$K_{11}: 89 \pm 2.8$ $K_{12}: 1.7 \pm 0.1$	110 ± 5.9		99 ± 5.7	$K_{11}: 110 \pm 7.7$ $K_{12}: 2.0 \pm 0.4$
 <b>7</b>	100 ± 5.5	$K_{11}: 210 \pm 8.8$ $K_{12}: 23 \pm 0.6$	80 ± 3.8		110 ± 4.2	
 <b>8</b>	74 ± 3.6	$K_{11}: 160 \pm 13$ $K_{12}: 2.1 \pm 0.2$	83 ± 3.6	$K_{11}: 130 \pm 11$ $K_{12}: 0.5 \pm 0.08$	58 ± 2.4	
 <b>9</b>	160 ± 11		61 ± 1.2	$K_{11}: 430 \pm 29$ $K_{12}: 100 \pm 3.9$	70 ± 2.5	$K_{11}: 120 \pm 4.8$ $K_{12}: 0.7 \pm 0.04$
 <b>10</b>	320 ± 28		140 ± 14		230 ± 18	
 <b>11</b>	1600 ± 290		720 ± 74		440 ± 26	
 <b>12</b>	1800 ± 360		540 ± 64		490 ± 27	$K_{11}: 680 \pm 37$ $K_{12}: 120 \pm 7.6$
 <b>13</b>	18 ± 0.7		77 ± 3.2		86 ± 5.2	$K_{11}: 76 \pm 4.0$ $K_{12}: 0.5 \pm 0.05$
 <b>14</b>	120 ± 9.2	$K_{11}: 49 \pm 2.7$ $K_{12}: 4.8 \pm 0.4$	100 ± 9.1		79 ± 3.8	

<sup>a</sup> in  $\text{CH}_3\text{CN}$ , [**1-3**] = 1.0  $\mu\text{M}$ , absorbance changes measured at 325nm and 365 nm.

As can be seen in Table 1, the affinity of these neutral species for cages **1-3** is high, ranging from 18000  $\text{M}^{-1}$  (naphthoic acid in **1**, to  $1.8 \times 10^6 \text{ M}^{-1}$  (adamantanol **12** in cage **1**). The properties of the carbazole cage mimic those of fluorene cage **4**, in that several guests show affinities that can be well fit to a non-cooperative 1:2 model, forming homoternary complexes. Anthracene **6**, anthraquinone **7** and 2,7-dibromofluorene **8** all favor 1:2 binding in **1**, although the larger 2,7-dibromofluorenyl ester **9** does not; obviously, very large guests cannot both fit inside the cavity of **1**. The 1:1 affinity for the larger guests (octanethiol **10** and the fluorenyl ester **9**) is larger than the equivalent 1:1  $K_a$  for the smaller guests that can also form ternary complexes, which again is consistent: larger guests show better space-filling in a 1:1 mode than smaller guests that bind in a 1:2 fashion. Interestingly, the strongest affinity is shown by the spherical adamantanone **11** and adamantanol **12**, which only form 1:1 complexes (the 1:2 fit was extremely poor), yet bind with affinities  $> 10^6 \text{ M}^{-1}$ . For comparison, the affinities ( $K_a$ , 1:1) of adamantanol and adamantanone in cage **4** are  $7.4 \times 10^5 \text{ M}^{-1}$  and  $1.2 \times 10^5 \text{ M}^{-1}$  respectively, showing that the carbazole cage **1** binds these targets  $\sim 5$ - $10\times$  more strongly.

Functionalized cages **2** and **3** can also bind these guests strongly, although the affinities are slightly lower than those shown by **1**. The internal thioether groups in cage **2** are quite inert, and only cause a small change in target affinity for simple neutral species due to space-filling effects. If there are any favorable interactions with H-bond donating guests, the effects are small. Most notably, these more "packed" cages displayed a lesser preference for 1:2 binding than in **1**, which is consistent with a reduction in cavity space due to the presence of the six ethylthiomethyl and ethyldimethylamino groups in the cavities of **2** and **3**, respectively. In the case of **2**, all guests tested showed very high ( $>>10\%$ ) errors in fitting to a 1:2 model, with the unexpected exception of the two dibromofluorene guests **8** and **9** (Table 1). The errors in those cases are not high enough to exclude the possibility of ternary complex formation, although the 1:2 fits are no better than the 1:1 model; we include them here for completeness.

The more basic amines in cage **3** have a much greater effect on the molecular recognition. The first point to note (Figure 7a,b) is that cage **3** is a robust host, capable of binding all nine guests tested, with affinities ranging from 58000  $\text{M}^{-1}$  (guest **8**),

to  $1.1 \times 10^6 \text{ M}^{-1}$  (adamantanol). This is in stark contrast to fluorenyl ammonium cage **5**, which displays a “blocked” cavity and does not bind neutral guest molecules. It had been previously shown that ester **9** shows no affinity for cage **5**,<sup>9d</sup> as can be seen in Figure 7b and ESI Figure S-56, neither naphthoic acid **13** nor anthracene **6** show any affinity for cage **5** either. In contrast, amine cage **3** not only binds naphthoic acid **13** strongly ( $1:1 K_a = 86000 \text{ M}^{-1}$ , Figure 7a and Table 1), but it can even form homoternary complexes with it. In this case, the errors in fitting for the 1:2 model are lower than the 1:1; this, coupled with the clear preference for binding the larger anthroic acid **14** in a 1:1 manner, shows the effect of more basic groups on the cage interior. The other non-acidic guests generally favored 1:1 binding with affinities similar to those with cage **2**; 1:2 binding between guests **6** and **9** and amine cage **3** could not be ruled out by model fitting, but 1:1 binding is more likely.

This data illustrates the major difference between **3** and **5** (and reinforces the MS/NMR data): cage **5** forms with 12 protonated amines on the cavity interior, which are paired with a corresponding number of  $\text{ClO}_4^-$  ions in the cavity to balance the charge. This prevents neutral guest binding (and provides supporting evidence for the location of guests when bound to other cages of this type: blocking the cavity removes any guest affinity, so species such as anthracene **6**, etc., must be bound on the cavity interior of **1-3**, as opposed to simply interacting with the external surface, as has been shown for other Fe-iminopyridine cages<sup>15</sup>). In contrast, while some protonation of the internal amines in **3** is plausible, it is far weaker and far less complete than in **5**, likely with  $\sim 1-3$  amines protonated at maximum, and with no corresponding bound  $\text{NTf}_2^-$  ions in the cavity that would block guest recognition. The favorable affinity of large acids suggests that the protonation of the internal amines is not complete, and does not repel the acid groups in **13** or **14**.

Obviously, UV titrations of acids and bases into amine cage **3** (as opposed to the more inert **1,2**) have a drawback: the change in UV absorption is not a robust method of differentiating between host:guest binding and protonation/deprotonation of the internal amines. While neutral small molecules should have no effect on the amine protonation state in **3**, acids such as **13**, **14**, mesic acid or pivalic acid, or bases such as DABCO could affect the internal amines, changing the absorbance spectrum from simple acid-base chemistry, rather than occurring from host:guest binding. As such, we titrated mesic acid, pivalic acid and DABCO into a  $\text{CD}_3\text{CN}$  solution of **3** and monitored the changes in both cage and additive by  $^1\text{H}$  NMR (see Figure 7c for DABCO, and ESI Figures S-63 and S-64 for pivalic acid). The strong mesic acid caused rapid degradation of cage **3**, even at only 2 mol.-eq. acid, so was not studied further. Pivalic acid, on the other hand, was highly well-tolerated, with no decomposition observed. More interestingly, there was no change at all in any of the cage **3** peaks, even those for the internal  $\text{NMe}_2$  residues at 2.8-2.9 ppm. The pivalic acid methyl group also showed zero change in shift upon addition. This lack of interaction (either by binding or protonation) supports the notion that naphthoic binds in cage **3** (Figure 7a) rather than simply protonating the internal amines.

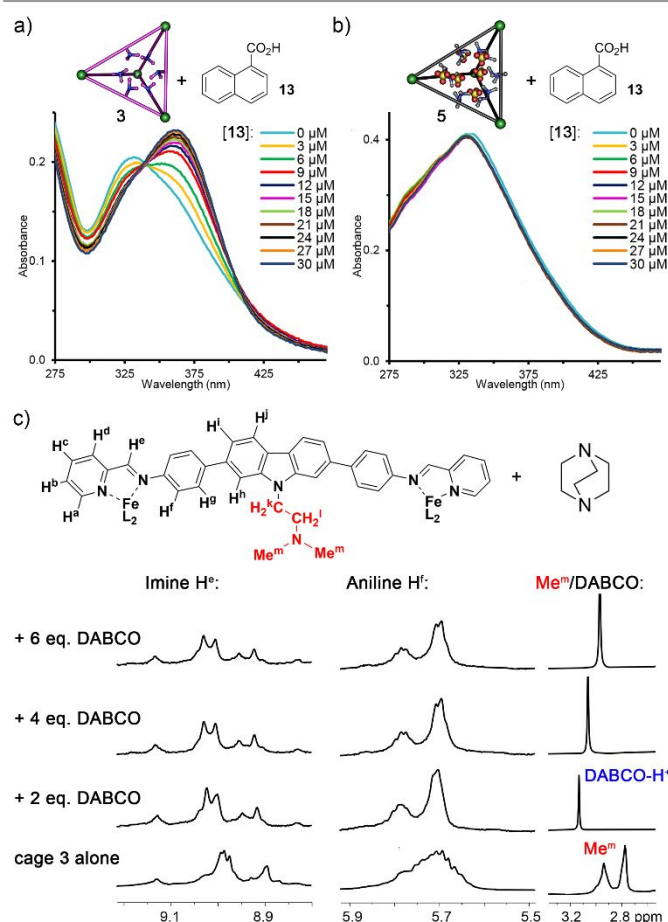


**Figure 7.** Variable molecular recognition properties of amine cage **3** vs. ammonium cage **5**. UV-Vis spectra upon titration of naphthoic acid **13** into a) cage **3**; b) cage **5**. c) Expansions of the  $^1\text{H}$  NMR spectra of cage **3** upon addition of excess DABCO ( $\text{CD}_3\text{CN}$ , 400 MHz methyl peaks  $\text{Me}^m$  shift upfield upon DABCO addition and are obscured by exogenous water; see ESI for full spectra).

This rather surprising observation was explained upon observing the effect of adding of DABCO to cage **3** (Figure 7c). The imine proton ( $\text{H}^e$ ) and ortho-aniline proton  $\text{H}^f$  regions of the  $^1\text{H}$  NMR spectrum sharpen considerably after addition of only one equivalent of 2 mol.-eq DABCO, and the  $\text{NMe}_2$  peaks shift abruptly upfield to  $\sim 2.2$  ppm (which overlaps with exogenous water signal in the  $\text{CD}_3\text{CN}$ ). The peak for added DABCO resides at 3.0 ppm, which is very close to the shift shown by protonated  $\text{DABCO-H}^+$  in  $\text{CD}_3\text{CN}$ .<sup>9d</sup> Addition of excess DABCO causes little more change in cage peaks, but the DABCO peak moves closer to that of free DABCO (2.7 ppm). The amine cage **3** is far less tolerant to added base than the fluorenyl counterpart **5**<sup>9d</sup> – upon addition of  $>6$  eq. DABCO, significant cage decomposition is observed (see ESI). Evidently, cage **3** does exist as an ammonium salt in solution, but the protonation state is far more fluid than in **5**: the protons are freely exchanging and do not occupy all the  $\text{NMe}_2$  sites in the cavity, causing broadening of the  $^1\text{H}$  NMR signals in the cage. Once a mild base is added, these protons are removed, and the spectrum of **3** becomes sharp, and significantly more reminiscent of that shown by the inert carbazole/thioether cages **1/2**. Addition of DABCO also

caused a slight lowering of the emission intensity of cage **3** (see ESI). This lowering was not dependent on DABCO concentration, suggesting that the quenching is not due to intermolecular interactions, but that the added base further deprotonates the internal  $\text{NMe}_2\text{H}^+$  groups, causing additional quenching.

## Conclusions

Here, we have shown that self-assembled cage  $\text{Fe}_4\text{L}_6$  complexes with variable internal functions can be synthesized using a 2,7-dibromocarbazole scaffold. The carbazole ligand allows internalization of six functional groups to the cage interior, and both ethylthiomethylether and ethyldimethylamino groups can be incorporated. The unfunctionalized cage **1** and the thioether cage **2** are quite similar in structure and properties, and show strong ligand-centered fluorescence emission and a broad range of guest binding properties; the larger cavity in cage **1** is capable of coencapsulation of neutral organic guests, whereas the thioether has a more sterically hindered cavity that favors 1:1 guest binding. In/out exchange is rapid, and binding affinities  $K_a$  up to  $10^6 \text{ M}^{-1}$  in  $\text{CH}_3\text{CN}$  are seen. The dimethylamino cage **3** is more complex, and the internal amines display partial protonation. The cage is mildly acidic, and shows no reaction with weak acids, but can be deprotonated by amine bases. In contrast to the previously reported fluorene variant **5**, however, the cavity is not blocked by counterions, allowing a broad range of neutral organic substrates to be bound, with affinities and stoichiometries comparable to that of the similarly sized thioether cage **2**. The amino groups alter the emission intensity, as the unprotonated lone pairs quench the ligand-centered emission. Overall, this is a flexible system that allows incorporation of variable internal functions and tuning of the cage properties, which is important for expanding the scope of these functionalized cages in areas such as catalysis, selective molecular recognition and sensing. Further studies of this system are underway in our laboratory.

## Experimental

### General Information

Cages **4**<sup>9a</sup> and **5**<sup>9d</sup> were synthesized according to literature procedures. 2,7-Dibromocarbazole, 4-Boc-aminophenylboronic acid, pyridine carboxaldehyde, cesium carbonate, palladium acetate, tricyclohexylphosphine were purchased from ChemScene, Acros Organics, or CombiBlocks and used as received. All other materials were obtained from Aldrich Chemical Company (St. Louis, MO) or Fisher Scientific (Fair Lawn, NJ) and used as received.  $^1\text{H}$  and  $^{13}\text{C}$  spectra were recorded on a Bruker Avance NEO 400 MHz or Bruker Avance 600 MHz NMR spectrometer. The spectrometers were automatically tuned and matched to the correct operating frequencies. Proton ( $^1\text{H}$ ) and carbon ( $^{13}\text{C}$ ) chemical shifts are reported in parts per million ( $\delta$ ) with respect to tetramethylsilane (TMS,  $\delta = 0$ ) and referenced internally with respect to the protio solvent impurity for  $\text{CD}_3\text{CN}$  ( $^1\text{H}$ : 1.94 ppm,  $^{13}\text{C}$ : 118.3 ppm) or  $\text{DMSO}-d_6$  ( $^1\text{H}$ : 2.54 ppm,  $^{13}\text{C}$ : 40.45).

Deuterated NMR solvents were obtained from Cambridge Isotope Laboratories, Inc. (Andover, MA) and used without further purification. Spectra were digitally processed (phase and baseline corrections, peak analysis, integration) using Bruker Topspin 1.3 and MestreNova. Solvents were dried with a commercial solvent purification system (Pure Process Technologies, Inc.). UV/vis spectroscopy was performed on a Cary 60 Photospectrometer with the Varian Scans program to acquire data. Fluorescence spectra were taken on a Horiba PTI QM-400 Fluorescence spectrophotometer. The mass spectrometric sample of cages **1-3** was prepared in 100% MeCN and infused into an Orbitrap Velos Pro mass spectrometer (Thermo Fisher Scientific, San Jose, CA, USA) with a homebuilt nanoESI source. The spray voltage, capillary temperature, and the S-lens RF level were set to 1.7 kV, 160 °C, and 45% respectively. Full mass spectra were acquired with a resolution of  $r = 30\,000$ . Thermo Xcalibur was used to analyze MS data and prepare the predicted isotope patterns. For all other molecules, high resolution accurate mass spectral data were obtained from the Analytical Chemistry Instrumentation Facility at the University of California, Riverside, on an Agilent 6545 QTOF LC/MS instrument.

### Synthesis and Characterization of New Molecules

**4,4'-(9H-Carbazole-2,7-diyl)dianiline (L1).** Cesium carbonate (4.40 g, 13.5 mmol), 2,7-dibromo-9H-carbazole **A** (750 mg, 2.25 mmol), 4-Boc-aminophenyl boronic acid (1.33 g, 5.63 mmol), palladium acetate (25.2 mg, 0.112 mmol), and tricyclohexylphosphine (63.1 mg, 0.225 mmol) were added to a two-neck round-bottom flask. The flask was then purged with  $\text{N}_2$  and 8 mL of isopropanol and 4 mL of toluene were added. The reaction mixture was stirred at 90 °C for 24 h. The mixture was then allowed to cool to room temperature and extracted with 10 mL of water and 4 x 50 mL of diethyl ether. The organic layer was filtered through Celite and the filtrate washed with a solution of 1 M sorbitol in water, saturated sodium bicarbonate, and brine (3 x 25 mL each). The organic layer was then dried with sodium sulfate and the solvent was removed in vacuo until minimal diethyl ether remained. Hexanes (30 mL) were added to precipitate the product di-tert-butyl ((9H-carbazole-2,7-diyl)bis(4,1-phenylene))-dicarbamate, which was collected via vacuum filtration before purification with silica column chromatography (0–10% EtOAc/hexanes) to yield a tan solid (519 mg, 42%).  $^1\text{H}$  NMR (600 MHz,  $\text{DMSO}-d_6$ )  $\delta$  11.36 (s, 1H), 9.49 (s, 2H), 8.15 (d,  $J = 8.1$  Hz, 2H), 7.70–7.65 (m, 6H), 7.59 (d,  $J = 8.3$  Hz, 4H), 7.44 (dd,  $J = 8.1, 1.6$  Hz, 2H), 1.52 (s, 18H).  $^{13}\text{C}$  NMR (150 MHz,  $\text{DMSO}-d_6$ )  $\delta$  152.80, 140.98, 138.76, 137.47, 134.78, 127.09, 121.23, 120.51, 118.51, 117.58, 108.26, 79.09, 28.16. HRMS (ESI-TOF)  $m/z$  calcd for  $\text{C}_{34}\text{H}_{35}\text{N}_3\text{O}_4$  ( $[\text{M} - \text{H}]^-$ ): 549.2628; found 549.2636.

The Boc-protected carbazole (200 mg, 0.36 mmol) was placed in a round-bottom flask and trifluoroacetic acid (4 mL, neat) was added. The mixture was stirred overnight at room temperature. The reaction mixture was then slowly added to a beaker containing 50 mL of saturated sodium bicarbonate solution. The solution was then brought to pH 12 using 2 M NaOH, and the precipitate filtered and washed with hexanes and sodium bicarbonate to yield ligand **L1** as a brown solid (93.1 mg, 42%).



$^1\text{H}$  NMR (600 MHz, DMSO- $d_6$ )  $\delta$  11.14 (s, 1H), 8.04 (d,  $J$  = 8.1 Hz, 2H), 7.56 (d,  $J$  = 1.6 Hz, 2H), 7.47 – 7.42 (m, 4H), 7.35 (dd,  $J$  = 8.1, 1.6 Hz, 2H), 6.71 – 6.66 (m, 4H), 5.23 (s, 4H).  $^{13}\text{C}$  NMR (150 MHz, DMSO- $d_6$ )  $\delta$  148.07, 140.96, 138.24, 128.57, 127.42, 120.57, 120.11, 117.01, 114.30, 107.19. HRMS (ESI-TOF)  $m/z$  calcd for  $\text{C}_{24}\text{H}_{19}\text{N}_3$  ( $[\text{M} - \text{H}]^-$ ): 349.1579; found 349.1593.

**Carbazole cage (1).** Ligand **L1** (56 mg, 0.16 mmol) was placed in a round-bottom flask with dry acetonitrile (12 mL) and heated to 80 °C, followed by the addition of 2-formylpyridine (28.8  $\mu\text{L}$ , 34.2 mg, 0.32 mmol). The reaction mixture was stirred for 10 minutes, then iron (II) triflimide (66 mg, 0.10 mmol) was added. The flask was then purged with  $\text{N}_2$ , and the reaction mixture stirred at 80 °C for 24 hours. The solution was allowed to cool, and any remaining solids were removed via vacuum filtration. The acetonitrile was removed in vacuo, and the remaining solid dissolved in 0.5 mL acetonitrile. The solid was then precipitated out with the addition of 15 mL diethyl ether and sonicated briefly, followed by filtration to afford a dark red solid as the product cage **1** (84.2 mg, 52%). For full spectra and characterization, see ESI.

**2,7-dibromo-9-(2-(methylthio)ethyl)-9H-carbazole (B).** To a two-neck round-bottom flask, 2,7-dibromocarbazole (1.0 g, 3.1 mmol), tetrabutylammonium hydrogen sulfate (41.7 mg, 0.12 mmol), sodium hydroxide (443 mg, 11.1 mmol) were added. The flask was then purged with  $\text{N}_2$  and 2-chloroethyl methyl sulfide (340  $\mu\text{L}$ , 3.3 mmol) and 7 mL acetonitrile were added. The mixture was stirred at reflux for 16 hours before being allowed to cool to room temperature. The resulting precipitate was isolated via vacuum filtration and washed with minimal acetonitrile. The product was then purified by silica column chromatography (10% EtOAc/hexanes) to afford the product as a white solid (1.12 g, 91%).  $^1\text{H}$  NMR (400 MHz, DMSO- $d_6$ )  $\delta$  8.13 (d,  $J$  = 8.2 Hz, 2H), 7.94 (d,  $J$  = 1.7 Hz, 2H), 7.38 (dd,  $J$  = 8.2, 1.7 Hz, 2H), 4.63 (t,  $J$  = 6.9 Hz, 2H), 2.90 (t,  $J$  = 6.9 Hz, 2H), 2.05 (s, 3H).  $^{13}\text{C}$  NMR (150 MHz, DMSO- $d_6$ )  $\delta$  141.09, 122.38, 122.18, 120.79, 119.16, 112.70, 32.22, 25.49, 15.05. HRMS (ESI-TOF)  $m/z$  calcd for  $\text{C}_{15}\text{H}_{13}\text{Br}_2\text{NS}$  ( $[\text{M} + \text{H}]^+$ ): 396.9135; found 396.9116.

**4,4'-(9-(2-(methylthio)ethyl)-9H-carbazole-2,7-diyl)dianiline (L2).** Thioether **B** (798 mg, 2.0 mmol), 4-Boc-aminophenyl boronic acid (1.19 g, 5 mmol), cesium carbonate (3.91 g, 12 mmol), and [1,1'-Bis(diphenylphosphino)ferrocene] dichloro-palladium(II) (146 mg, 0.2 mmol) were added to a two-neck round-bottom flask. The flask was purged with  $\text{N}_2$  and 4 mL of dry dimethylformamide was added. The reaction mixture was stirred at 85 °C for 24 hours and allowed to cool. The product was extracted with 5 mL of water and diethyl ether (4 x 50 mL). The organic layer was filtered through Celite and washed with 1 M sorbitol in water, saturated sodium bicarbonate, and brine (3 x 25 mL each). The organic layer was then dried with sodium sulfate and the solvent was removed in vacuo until minimal diethyl ether remained. Hexanes (30 mL) were added to precipitate the product, which was collected via vacuum filtration. The solid was then purified using silica column chromatography (0–6% EtOAc/hexanes) yielding di-tert-butyl ((9-(2-(methylthio)ethyl)-9H-carbazole-2,7-diyl)bis(4,1-phenylene))dicarbamate as a beige solid (598 mg, 48%).  $^1\text{H}$  NMR (400 MHz, DMSO- $d_6$ )  $\delta$  9.46 (s, 2H), 8.17 (d,  $J$  = 8.2 Hz, 2H), 7.85 (d,  $J$

= 1.5 Hz, 2H), 7.78 – 7.71 (m, 4H), 7.60 (d,  $J$  = 8.4 Hz, 4H), 7.49 (dd,  $J$  = 8.2, 1.5 Hz, 2H), 4.75 (t,  $J$  = 7.2 Hz, 2H), 3.04 – 2.94 (m, 2H), 2.13 (s, 3H), 1.51 (s, 18H).  $^{13}\text{C}$  NMR (150 MHz, DMSO- $d_6$ )  $\delta$  152.77, 141.13, 138.83, 137.66, 134.72, 127.29, 120.93, 120.55, 118.42, 117.88, 106.83, 79.10, 32.34, 28.15, 15.08. HRMS (ESI-TOF)  $m/z$  calcd for  $\text{C}_{37}\text{H}_{41}\text{N}_3\text{O}_4\text{S}$  ( $[\text{M} - \text{H}]^-$ ): 623.2818; found 623.2836.

The Boc-protected thioether (400 mg, 0.64 mmol) was placed in a round-bottom flask and trifluoroacetic acid (6 mL, neat) was added, then stirred for 24 hours at room temperature. The reaction mixture was then slowly added to a beaker containing 50 mL of saturated sodium bicarbonate solution. 2M NaOH was used to basify the solution to pH 12, resulting in a precipitate forming. This was then filtered and washed with sodium bicarbonate to yield ligand **L2** as a tan solid (163 mg, 60%).  $^1\text{H}$  NMR (600 MHz, DMSO)  $\delta$  8.07 (d,  $J$  = 8.2 Hz, 2H), 7.72 (s, 2H), 7.53 (d,  $J$  = 8.1 Hz, 4H), 7.39 (d,  $J$  = 8.1 Hz, 2H), 6.70 (d,  $J$  = 8.1 Hz, 4H), 5.25 (s, 4H), 4.71 (t,  $J$  = 7.0 Hz, 2H), 2.98 (t,  $J$  = 7.0 Hz, 2H), 2.13 (s, 3H).  $^{13}\text{C}$  NMR (600 MHz, DMSO)  $\delta$  147.39, 141.05, 138.29, 128.97, 127.59, 120.24, 120.12, 117.26, 114.58, 105.76, 32.28, 26.99, 15.04. HRMS (ESI-TOF)  $m/z$  calcd for  $\text{C}_{27}\text{H}_{25}\text{N}_3\text{S}$  ( $[\text{M} + \text{H}]^+$ ): 423.1769; found 423.1758.

**Thioether Cage (2).** Ligand **L2** (33.9 mg, 0.08 mmol) and 2-formylpyridine (14.4  $\mu\text{L}$ , 17.1 mg, 0.16 mmol) were placed in a round-bottom flask with 6 mL dry acetonitrile and stirred at reflux for 10 minutes. Iron (II) triflimide (66 mg, 0.10 mmol) was added and the flask purged with  $\text{N}_2$ . The mixture was then stirred at reflux for 24 hours and allowed to cool. Remaining solids were removed via vacuum filtration, and the acetonitrile was removed in vacuo. The resulting solid was dissolved in 0.5 mL acetonitrile, then precipitated out with the addition of 15 mL diethyl ether and sonicated briefly. Vacuum filtration was performed to afford a dark red solid as the product cage **2** (51.0 mg, 63%). For full spectra and characterization, see ESI.

**2-(2,7-dibromo-9H-carbazol-9-yl)-N,N-dimethylethanamine (C).** To a two-neck round-bottom flask 2,7-dibromocarbazole (1.0 g, 3.1 mmol), dimethylaminoethyl chloride hydrochloride (480 mg, 3.3 mmol), tetrabutylammonium hydrogen sulfate (41.7 mg, 0.12 mmol), sodium hydroxide (443 mg, 11.1 mmol) were added. Acetonitrile (5 mL) was added after the flask was purged with  $\text{N}_2$ . After stirring at reflux overnight, the solution was allowed to cool to room temperature. The resulting solid was then isolated via vacuum filtration and washed with minimal acetonitrile before purification via silica column chromatography (10% EtOAc/hexanes) to afford a light brown solid as the product (1.06 mg, 86%).  $^1\text{H}$  NMR (600 MHz, DMSO- $d_6$ )  $\delta$  8.14 (d,  $J$  = 8.2 Hz, 2H), 7.89 (d,  $J$  = 1.8 Hz, 2H), 7.37 (dd,  $J$  = 8.2, 1.8 Hz, 2H), 4.50 (t,  $J$  = 6.5 Hz, 2H), 2.59 (t,  $J$  = 6.5 Hz, 2H), 2.20 (s, 6H).  $^{13}\text{C}$  NMR (150 MHz, DMSO- $d_6$ )  $\delta$  141.39, 122.44, 122.35, 120.94, 119.34, 112.73, 57.32, 45.64, 41.11. HRMS (ESI-TOF)  $m/z$  calcd for  $\text{C}_{16}\text{H}_{16}\text{Br}_2\text{N}_2$  ( $[\text{M} + \text{H}]^+$ ): 393.9680; found 393.9678.

**4,4'-(9-(2-(dimethylamino)ethyl)-9H-carbazole-2,7-diyl)-dianiline (L3).** Amino-carbazole **C** (790 mg, 2.0 mmol), 4-Boc-aminophenyl boronic acid (1.19 g, 5 mmol), cesium carbonate (3.91 g, 12 mmol), and [1,1'-Bis(diphenylphosphino)ferrocene] dichloro-palladium(II) (146 mg, 0.2 mmol) were added to a two-

neck round-bottom flask. The flask was purged with N<sub>2</sub> and 4 mL of dry isopropanol and 2 mL toluene were added. The reaction mixture was stirred at 90°C for 24 hours and allowed to cool. The product was extracted with 5 mL of water and diethyl ether (4 x 50 mL). The organic layer was filtered through Celite and washed with 1 M sorbitol in water, saturated sodium bicarbonate, and brine (3 x 25 mL each). The organic layer was then dried with sodium sulfate and the solvent was removed in vacuo until minimal diethyl ether remained. Hexanes (30 mL) were added to precipitate the product, which was collected via vacuum filtration. The product was then purified with silica column chromatography (0–6% EtOAc/hexanes) to yield di-tert-butyl ((9-(2-(dimethylamino)ethyl)-9H-carbazole-2,7-diyl)bis(4,1-phenylene))dicarbamate as a tan solid (598 mg, 48%). <sup>1</sup>H NMR (600 MHz, DMSO-*d*<sub>6</sub>) δ 9.49 (s, 2H), 8.18 (dd, *J* = 8.1, 4.1 Hz, 2H), 7.82 (d, *J* = 17.4 Hz, 2H), 7.74 (d, *J* = 8.6 Hz, 4H), 7.61 (d, *J* = 8.3 Hz, 4H), 7.49 (d, *J* = 8.6 Hz, 2H), 4.62 (t, *J* = 6.8 Hz, 2H), 2.69 (t, *J* = 6.8 Hz, 2H), 2.26 (s, 6H), 1.52 (s, 18H). <sup>13</sup>C NMR (100 MHz, DMSO-*d*<sub>6</sub>) δ 152.76, 141.28, 138.82, 137.61, 134.75, 127.24, 120.52, 118.44, 106.74, 79.07, 57.48, 45.59, 28.14. HRMS (ESI-TOF) *m/z* calcd for C<sub>38</sub>H<sub>44</sub>N<sub>4</sub>O<sub>4</sub> ([M + H]<sup>+</sup>): 620.3363; found 620.3350.

The Boc-protected amino ligand (400 mg, 0.64 mmol) was added to a round-bottom flask with trifluoroacetic acid (8 mL, neat). The mixture was stirred overnight at room temperature. The reaction mixture was then slowly added to a beaker containing 50 mL of saturated sodium bicarbonate solution. The solution was then basified to pH 12 using 2 M NaOH, and the precipitate filtered and washed with sodium bicarbonate to yield ligand **L3** as a brown solid (206 mg, 76%). <sup>1</sup>H NMR (400 MHz, CD<sub>3</sub>CN) δ 8.10 (dd, *J* = 8.1, 3.1 Hz, 2H), 7.66 (d, *J* = 1.6 Hz, 2H), 7.57 (dd, *J* = 8.5, 4.5 Hz, 4H), 7.44 (dd, *J* = 8.1, 1.6 Hz, 2H), 6.83–6.75 (m, 4H), 4.54 (t, *J* = 6.8 Hz, 2H), 4.28 (s, 4H), 2.77 (t, *J* = 6.8 Hz, 1H), 2.31 (s, 6H). <sup>13</sup>C NMR (100 MHz, DMSO-*d*<sub>6</sub>) δ 148.16, 141.26, 138.39, 128.57, 127.59, 120.16, 117.11, 114.26, 105.65, 57.46, 45.65, 40.55. HRMS (ESI-TOF) *m/z* calcd for C<sub>28</sub>H<sub>28</sub>N<sub>4</sub> ([M + H]<sup>+</sup>): 420.2314; found 420.2310.

**Amine cage (3).** Ligand **L3** (34.4 mg, 0.08 mmol) and 2-formylpyridine (16 μL, 18.2 mg, 0.17 mmol) were placed in a round-bottom flask with 16 mL dry acetonitrile and stirred at reflux for 15 minutes. Iron (II) triflimide (68 mg, 0.11 mmol) was added and the flask purged with N<sub>2</sub>. The mixture was then stirred at 50 °C for 24 hours and allowed to cool. Remaining solids were removed via vacuum filtration, and the acetonitrile was removed in vacuo. The resulting solid was dissolved in 0.5 mL acetonitrile, then precipitated out with the addition of 15 mL diethyl ether and sonicated briefly. Vacuum filtration was performed to afford a dark red solid as the product cage **3** (57.5 mg, 71%). For full spectra and characterization, see ESI.

## Conflicts of interest

There are no conflicts to declare.

## Acknowledgements

The authors would like to thank the National Science Foundation (CHE-2002619 to R.J.H.; CHE-1904577 to R.R.J.) for support.

## Notes and references

- 1 a) M. D. Ward and P. R. Raithby, *Chem. Soc. Rev.* 2013, **42**, 1619–1636; b) N. J. Young and B. P. Hay, *Chem. Commun.* 2013, **49**, 1354–1379; c) T. R. Cook and P. J. Stang, *Chem. Rev.* 2015, **115**, 7001–7045; d) M. M. J. Smulders, I. A. Riddell, C. Browne, J. R. Nitschke, *Chem. Soc. Rev.*, 2013, **42**, 1728–1754.
- 2 a) F. J. Rizzuto, L. K. S. von Krbeke and J. R. Nitschke, *Nat. Rev. Chem.* 2019, **3**, 204–222; b) R. Custelcean, P. V. Bonnesen, N. C. Duncan, X. Zhang, L. A. Watson, G. Van Berkel, W. B. Parson, B. P. Hay, *J. Am. Chem. Soc.* 2012, **134**, 8525–8534; c) D. Zhang, T. K. Ronson, J. Mosquera, A. Martinez, L. Guy, J. R. Nitschke, *J. Am. Chem. Soc.* 2017, **139**, 6574–6577; d) L.-J. Wang, X. Li, S. Bai, Y.-Y. Wang, Y.-F. Han, *J. Am. Chem. Soc.* 2020, **142**, 2524–2531; e) N. Kishi, Z. Li, K. Yoza, M. Akita, M. Yoshizawa, *J. Am. Chem. Soc.* 2011, **133**, 11438–11441; f) X. Jing, C. He, Y. Yang, C. Duan, *J. Am. Chem. Soc.* 2015, **137**, 3967–3974.
- 3 a) C. J. Brown, F. D. Toste, R. G. Bergman and K. N. Raymond, *Chem. Rev.* 2015, **115**, 3012–3035; b) C. M. Hong, R. G. Bergman and K. N. Raymond, *Acc. Chem. Res.* 2018, **51**, 2447–2455; c) I. Sindha and P. S. Mukherjee, *Inorg. Chem.* 2018, **57**, 4205–4221.
- 4 a) A. B. Grommet, J. L. Bolliger, C. Browne, C.; and J. R. Nitschke, *Angew. Chem., Int. Ed.* 2015, **54**, 15100–15104; b) A. B. Grommet and J. R. Nitschke, *J. Am. Chem. Soc.* 2017, **139**, 2176–2179; c) D. Zhang, T. K. Ronson, J. Mosquera, A. Martinez, J. R. Nitschke, *Angew. Chem. Int. Ed.* 2018, **57**, 3717–3721.
- 5 a) X. Yan, T. R. Cook, P. Wang, F. Huang and P. J. Stang, *Nat. Chem.* 2015, **7**, 342–348; b) Q.-W. Zhang, D. Li, X. Li, P. B. White, J. Mecinović, X. Ma, H. Ågren, R. J. M. Nolte, and H. Tian *J. Am. Chem. Soc.* 2016, **138**, 13541–13550; c) M. Zhang, M. L. Saha, M. Wang, Z. Zhou, B. Song, C. Lu, X. Yan, X. Li, F. Huang, S. Yin, and P. J. Stang *J. Am. Chem. Soc.* 2017, **139**, 5067–5074; d) Z. Zhang, Z. Zhao, L. Wu, S. Lu, S. Ling, G. Li, L. Xu, L. Ma, Y. Hou, X. Wang, X. Li, G. He, K. Wang, B. Zou, and M. Zhang, *J. Am. Chem. Soc.* 2020, **142**, 2592–2600.
- 6 a) C. Walsh, *Enzymatic Reaction Mechanisms*; W. H. Freeman, 1979; b) A. Fersht, *Structure and mechanism in protein science: a guide to enzyme catalysis and protein folding*; Macmillan, 1999; c) W. P. Jencks, *Catalysis in Chemistry and Enzymology*; McGraw-Hill, 1969; d) A. J. Kirby, *Angew. Chem., Int. Ed. Engl.* 1996, **35**, 707–724.
- 7 P. M. Bogie, T. F. Miller and R. J. Hooley, *Isr. J. Chem.* 2019, **59**, 130–139.
- 8 a) K. Suzuki, J. Iida, S. Sato, M. Kawano, M. Fujita, *Angew. Chem. Int. Ed.* 2008, **47**, 5780–5782; b) K. Suzuki, M. Kawano, S. Sato, M. Fujita, *J. Am. Chem. Soc.* 2007, **129**, 10652–10653; c) Q.-Q. Wang, S. Gonell, S.H.A.M. Leenders, M. Dürr, I. Ivanović-Burmazović, J. N. H. Reek, *Nat. Chem.* 2016, **8**, 225–230; d) R. Gramage-Doria, J. Hessels, S.H.A.M. Leenders, O. Tröppner, M. Dürr, I. Ivanović-Burmazović, J. N. H. Reek, *Angew. Chem. Int. Ed.* 2014, **53**, 13380–13384; e) J. L. Bolliger, A. M. Belenguer, J. R. Nitschke, *Angew. Chem. Int. Ed.*, 2013, **52**, 7958–7962; f) Y. Ueda, H. Ito, D. Fujita, M. Fujita, *J. Am. Chem. Soc.* 2017, **139**, 6090–6093; g) D. Fujita, K. Suzuki, M. Yagi-Utsumi, Y. Yamaguchi, N. Mizuno, T. Kumasaka, M. Takata, M. Noda, S. Uchiyama, K. Kato, M. Fujita, *Nat. Commun.*, 2012, **3**, 1093–1099.
- 9 a) L. R. Holloway, P. M. Bogie, Y. Lyon, C. Ngai, T. F. Miller, R. R. Julian and R. J. Hooley, *J. Am. Chem. Soc.* 2018, **140**, 8078–8081; b) C. Ngai, C. M. Sanchez-Marsetti, W.H. Harman and R.

- J. Hooley, *Angew. Chem. Int. Ed.* 2020, **59**, 23505–23509; c) C. Ngai, B. da Camara, C. Z. Woods and R. J. Hooley, *J. Org. Chem.* 2021, **86**, 12862–12871. d) C. Ngai, H.-T. Wu, B. da Camara, C. G. Williams, L. J. Mueller, R. R. Julian and R. J. Hooley, *Angew. Chem. Int. Ed.* 2022, **61**, e202117011.
- 10 a) S. Zarra, J. K. Clegg and J. R. Nitschke, *Angew. Chem., Int. Ed.* 2013, **52**, 4837–4840; b) A. Jiménez, R. A. Bilbeisi, T. K. Ronson, S. Zarra, C. Woodhead and J. R. Nitschke, *Angew. Chem., Int. Ed.* 2014, **53**, 4556–4560; c) J. Mosquera, T. K. Ronson and J. R. Nitschke, *J. Am. Chem. Soc.* 2016, **138**, 1812–1815; d) A. J. McConnell, C. M. Aitchison, A. B. Grommet and J. R. Nitschke, *J. Am. Chem. Soc.* 2017, **139**, 6294–6297.
- 11 a) F.-R. Dai and Z. Wang, *Z. J. Am. Chem. Soc.* 2012, **134**, 8002–8005; b) Y. Qiao, L. Zhang, J. Li, W. Lin and Z. Wang, *Angew. Chem. Int. Ed.* 2016, **55**, 12778–12782.
- 12 T. J. Dale and J. Rebek, Jr. *J. Am. Chem. Soc.* 2006, **128**, 4500–4501.
- 13 C. Ngai, P. M. Bogie, L. R. Holloway, P. C. Dietz, L. J. Mueller and R. J. Hooley, *J. Org. Chem.* 2019, **84**, 12000–12008.
- 14 Association constants calculated using BindFit software found at <http://supramolecular.org>. a) P. Thordarson, *Chem. Soc. Rev.* 2011, **40**, 1305–1323; b) D. B. Hibbert, P. Thordarson, *Chem. Commun.* 2016, **52**, 12792–12805.
- 15 F. J. Rizzuto, J. P. Carpenter and J. R. Nitschke, *J. Am. Chem. Soc.* 2019, **141**, 9087–9095.